

Article

Effect of Magnesium Sulfate Solution on Pore Structure of Ionic Rare Earth Ore during Leaching Process

Zhongquan Gao ¹, Yunzhang Rao ^{1,*}, Liang Shi ², Run Xiang ¹ and Zhihua Yang ¹

¹ School of Resources and Environmental Engineering, Jiangxi University of Science and Technology, Ganzhou 341000, China

² School of Architectural and Surveying & Mapping Engineering, Jiangxi University of Science and Technology, Ganzhou 341000, China

* Correspondence: raoyunzhang@jxust.edu.cn; Tel.: +86-15083781770

Abstract: During in situ leaching of ionic rare earth ore, the pore structure of the orebody changes due to the chemical replacement reaction between the leaching agent and the rare earth ore. To explore the influence of leaching agents on the pore structure of ionic rare earth ore during the leaching process, magnesium sulfate solutions with different concentrations and pH are used as leaching agents in this paper. An experimental method of indoor simulated column leaching, a Zetaprobe potential analyzer, and an NM-60 rock microstructure analyzer to measure parameters, including surface zeta potential, T2 map, and the pore structure of rare-earth ore particles, were used to analyze the influence law of magnesium sulfate solution on the pore structure of ionic rare earth ore. The result proves that pure H₂O leaching has little effect on the surface Zeta potential and the internal pore structure of the ore particles. In the leaching process of magnesium sulfate solutions with different concentrations, the absolute value of Zeta potential decreases, and the internal pore structure evolves from medium, large, and extra-large to small pores. In the leaching process of magnesium sulfate solutions with different pH, the absolute value of Zeta potential decreases and then increases slightly with the end of the ion exchange reaction. The internal pore structure generally shows a decrease in the number of small and extra-large pores and an increase in the number of medium and large pores. According to the analysis, the concentration and pH of the leaching agent cause the change of thickness of the electric double layer of the fine particles in the orebody, break the balance of interaction force between soil particles, and result in the evolution of a micropore structure of orebody during leaching.

Keywords: ionic rare earth; leaching agent concentration and pH; electric double layer; pore structure



Citation: Gao, Z.; Rao, Y.; Shi, L.; Xiang, R.; Yang, Z. Effect of Magnesium Sulfate Solution on Pore Structure of Ionic Rare Earth Ore during Leaching Process. *Minerals* **2023**, *13*, 294. <https://doi.org/10.3390/min13020294>

Academic Editor: Kyoungkeun Yoo

Received: 23 December 2022

Revised: 2 February 2023

Accepted: 11 February 2023

Published: 20 February 2023



Copyright: © 2023 by the authors. Licensee MDPI, Basel, Switzerland. This article is an open access article distributed under the terms and conditions of the Creative Commons Attribution (CC BY) license (<https://creativecommons.org/licenses/by/4.0/>).

1. Introduction

Ionic rare earth ore, also known as ion-absorbed rare earth ore or weathered crust elution-deposited rare earth ore [1], is widely distributed in the Jiangxi, Fujian, Guangdong, Hunan, Guangxi, and other provinces in China. Rare earth elements are mainly adsorbed on the surface of clay minerals in the forms of hydrated cation(H₃O⁺) and hydroxyl hydrated cation(−OH). Rare earth elements are divided into light rare earth elements and medium-heavy rare earth elements. The latter are extensively used to manufacture permanent magnet materials, laser materials, superconducting materials, and electron devices [2–4]. After years of theoretical research and practical exploration, rare earth mining technology has developed from pond leaching to heap leaching to in situ leaching, which has the highest recovery rate of rare earth resources and mature technology [5]. The recovery rate and mining period of rare earth resources vary due to the different electrolyte type [6], concentration, pH [7], flow velocity of leaching agents, and liquid injection intensity [8,9] during in situ leaching. Meanwhile, solution permeability is affected by these factors as well. The pore structure of the orebody is changed and continuously evolves under the seepage effect. In the process of leaching, the structural stability of the orebody is constantly

changing, leading to slope instability, landslides, and other problems. Thus, studying the evolution of pore structure in the leaching process has great practical engineering guiding significance regarding the leaching effect of ionic rare earth ore and solutions for slope instability and landslides.

With the progress of technology [10,11], computed tomography (CT) has been applied to study the distribution characteristics of the micropore structure in particles. Many scientific researchers have conducted relevant theoretical research on the change in micropore structure [12,13]. Bezaatpour et al. [14] used the RCP algorithm to model porous media. The results showed that the predictive porosity is only 10% consistent with the observed measurements and that the consistency between pressure drop and permeability is good (up to 95%). Zhou et al. [1] studied the evolution features of pore structure in the leaching process with column leaching with different cationic leaching agents of NH_4^+ , Mg^{2+} , and Al^{3+} . The study indicated that the evolution of the pore structure of rare earth ore bodies induced by different valent cation leaching solutions is nearly similar. Wang et al. [15] analyzed the changing rules of the internal pore structure of rare earth during the leaching process of pure H_2O and $(\text{NH}_4)_2\text{SO}_4$ solutions with different concentrations. Experiments showed that during effective leaching time, compared with pure H_2O , the porosity and pore radius of orebody samples increase significantly in the leaching process of $(\text{NH}_4)_2\text{SO}_4$ solutions and become more obvious with the increase of solution concentration. Ion exchange causes the movement and recombination of particles and, thus, pore change [16]. Throughout the leaching process, ion exchange develops in layers along the direction of seepage. The microstructure of the orebody is affected alternately by physical seepage and ion exchange. Zhao et al. [17] proved that particle aggregation occurs when an NH_4Cl solution is used as a leaching agent. Under strong chemical reaction, soil microparticles separate from large particles and enter the solution, increasing porosity. The changing ionic strength changes the interaction force between soil particles (electrostatic repulsion, hydration repulsion, and van der Waals force) [18]. The blocked pore network slows the water entering the aggregate, thus changing the seepage direction. During the leaching process, rare earth particles disperse or condensate in different degrees due to different properties of Ca^{2+} or Mg^{2+} [19]. The dissolution of calcareous cement and the formation of clay minerals are inhibited by the cementation of Ca^{2+} [20]. The increase of electric potential on the surface of colloids and the decrease of electrostatic repulsion between particles make the soil structure stable. During the formation of clay particles [21], a diffused double layer with an electric field effect is formed on the particle surface [22], which effectively explains the interaction between clay compressibility and particle-water-cation [23]. The effect of the leaching agent cannot be ignored during the leaching process. Characteristic parameters like porosity, the torsion of capillary, and pore size distribution greatly influence orebody particles [24,25]. Crystal particles affect the pore size and pore throats and impact the pore structure of rare earth orebodies [26].

Most scholars have studied the evolution laws of internal seepage and pore structure of the orebody after leaching with different concentrations of ammonium sulfate solution. In this paper, magnesium sulfate solutions with different concentrations and pH are used as leaching agents. The chemical displacement reaction between Mg^{2+} and RE^{3+} in rare earth ore samples results in the breaking of the steady state of the interaction force between particles [27,28]. Then the change of electronic double layer thickness and pore structure of ionic rare earth orebody in the leaching process and the influence of magnesium sulfate solutions with different concentrations and pH on them are studied. The combination of microanalysis and macroanalysis provides a theoretical basis for further research and a solution for the evolution of pore structure in the leaching process.

2. Materials and Methods

2.1. Materials

The rare earth samples used in this paper were taken from Zudong rare earth deposit in Longnan County, Jiangxi province. The X-ray diffraction (XRD) patterns can be seen in

Figure 1. The oxides contained in the rare earth ore samples were Al_2O_3 (34.975%), SiO_2 (48.251%), Rb_2O (0.041%), Y_2O_3 (0.097%), Nd_2O_3 (0.031%), Yb_2O_3 (0.014%), and others (4.479%). The collected undisturbed soil was tested for particle gradation in the lab with screened particle sizes of 5, 2.5, 1, 0.5, and 0.075 mm in sequence. The screened soil particles were dried and weighed to calculate the mass fraction of each particle grade, as shown in Table 1. Magnesium sulfate solution was taken as the leaching agent in this experiment to conduct column leaching; six groups of magnesium sulfate solutions with different mass concentrations of 0.0%, 2.5%, 3.0%, 3.5%, 4.0%, and 4.5% were prepared; and 2.0% dilute sulfuric acid was used to prepare five groups of 3.5% magnesium sulfate solutions with different pHs of 2, 3, 4, 5, and 6. The magnesium sulfate particles used in this experiment were purchased from local chemical plants.

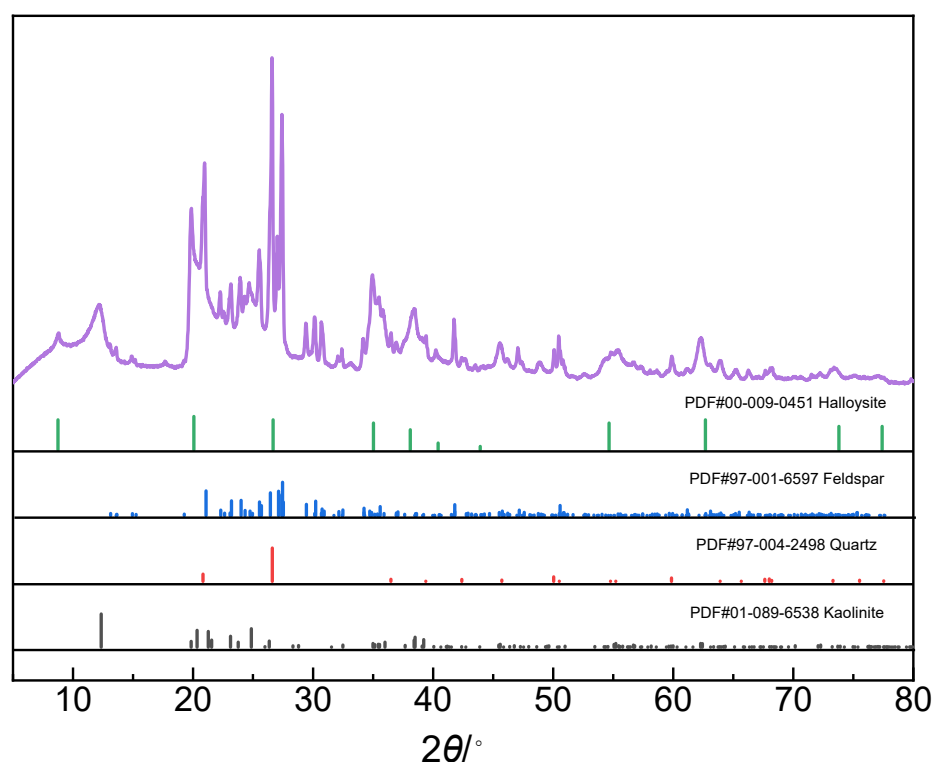


Figure 1. XRD pattern of run-of-mine ore sample.

Table 1. Particle gradation of undisturbed rare earth.

Particle Diameter (mm)	>5	2.5–5	1–2.5	0.5–1	0.075–0.5	<0.075
Percentage of interval (%)	12.8	28.9	7.3	8.4	28.7	13.9
percentage (%)	12.8	41.7	49.0	57.4	86.1	100

2.2. Experimental Method and Process

In this paper, the indoor simulated column leaching method of ionic rare earth ore was adopted and strictly implemented according to the standard of remolded soil samples. The device used for the indoor simulated column leaching test was an acrylic tube with an inner diameter of 44 mm and a wall thickness of 2 mm (Figure 2a). According to the effective range of the rock microstructure analyzer, the diameter–height ratio of the remolded soil sample was 44:60. During remolding, the soil samples were compacted in three layers. To avoid obvious stratification, each layer was roughened after compacting when preparing the samples. With the method of immersion saturation for initial saturation, the samples, completing 72 h of free water absorption in water, were taken out, and the surface was towed off. A group of samples with little difference in initial porosity and

saturation greater than 95% were selected to perform indoor column leaching. The effect of magnesium sulfate solutions with different concentrations and pH on the evolution of the pore structure of the orebody during leaching was studied using the indoor simulated column leaching method.

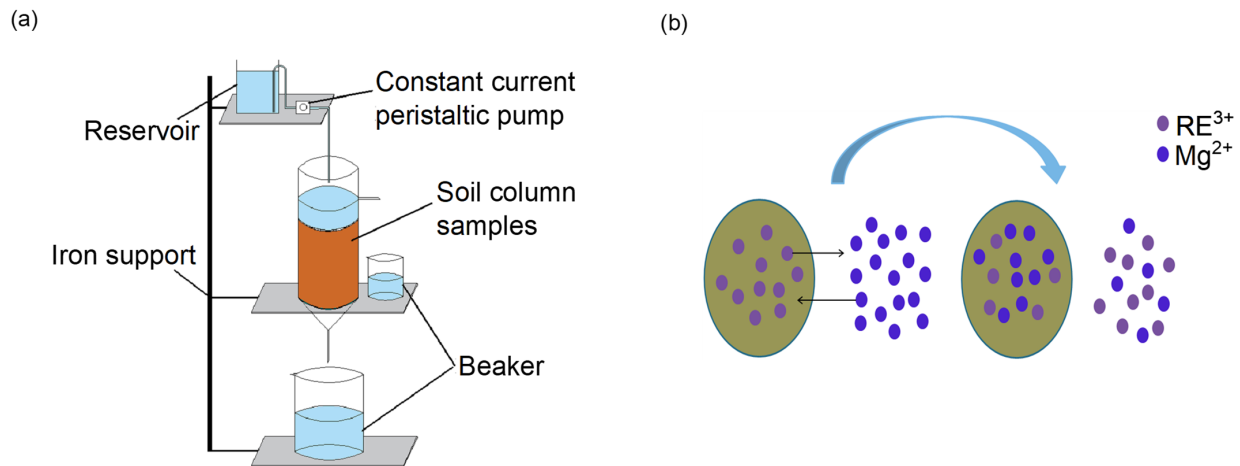


Figure 2. (a) Schematic diagram of experimental setup; (b) Rare earth leaching schematic.

In column leaching, the chemical reaction inside ionic rare earth is a dynamic desorption process, during which the Mg^{2+} in the solution and the RE^{3+} in the sample exchange ions (Figure 2b). The leaching mother liquor after leaching was collected and tested. According to the diffuse double layer theory, a Zetaprobe potential analyzer from Colloidal Dynamics, USA, was adopted to measure the Zeta potential of colloidal particles reflecting the adsorbed state of colloids and ions. An NM-60 magnetic resonance rock microstructure analyzer (Suzhou Niumag Analytical Instrument Corporation) was used to test the pore structure of the leaching samples. Before the experiment, the temperature of the permanent magnet inside the experimental instrument was adjusted and stabilized at $32\text{ }^{\circ}\text{C} \pm 0.1\text{ }^{\circ}\text{C}$. Using nuclear magnetic resonance analysis software Ver. 1.0 to test the micropore structure of the samples every 1h to quickly and precisely obtain porosity data, T2 map, pore size distribution, etc.

3. Results and Discussion

3.1. Effect of Concentration and pH of Leaching Agent on Zeta Potential of Rare Earth Ore Particles in Leaching Process

The surface of clay minerals, which is negatively charged, can adsorb the positively charged ions when contacting the solutions to maintain a stable state of electrical neutrality [29]. Thus, the concentration of positive charge on the clay mineral surface is higher than the bulk solution. Due to the cation concentration gradient, cations diffuse from the surface of clay minerals into the solution until the equilibrium between diffusion and attraction is reached, as shown in Figure 3.

Six groups of magnesium sulfate solutions with different mass percent concentrations of 0.0%, 2.5%, 3.0%, 3.5%, 4.0%, and 4.5% were prepared for the indoor column leaching test to measure the Zeta potential on the surface of rare earth particles and systematically analyze the influence of magnesium sulfate solutions with different concentrations on them. As shown in Figure 4, the rare earth sample leached with pure H_2O is relatively gentle in the value curve of Zeta potential, which is nearly a straight line, indicating that pure H_2O doesn't react with rare earth minerals in the leaching process and that RE^{3+} cannot be desorbed and thus has no influence on Zeta potential. When leaching with magnesium sulfate solutions with different concentrations, the absolute value of Zeta potential on the surface of rare earth particles decreased with the leaching time. The change of Zeta potential reached the maximum when the concentration of magnesium sulfate

solution was 4.0%, reduced by 53.60%. In the early leaching stage, the absolute value of Zeta potential on the particle surface tended to decrease. In the middle stage, the absolute value increased first and then decreased rapidly. After 3 h of leaching, the Zeta potential reached the maximum value. In 3–4 h, the value dropped sharply. In the later stage of leaching, the absolute value of samples leached with low concentrations of magnesium sulfate solutions decreased gradually, while the value of samples with high-concentration solutions presented an upward trend, and the overall change was relatively gentle. In the leaching process, the Zeta potential curve of the samples with high concentrations of magnesium sulfate solutions fluctuated greatly, while the change of samples with low-concentration solutions was relatively gentle. Since the surface of rare earth ore has strong hydrophobicity, the ore particles in the solution agglomerate and wrap the clay particles inside. This hinders the hydration of clay particles, resulting in a thinner electric double layer on the surface of particles. The absolute value of Zeta potential on the particle surface decreased in the early leaching stage. In the middle leaching stage, as the samples had gone through the preparing stage and initial reaction stage, the leaching agent had more time to react with the samples. The Mg^{2+} in the leaching agent reacted with the RE^{3+} in rare earth ore quickly to desorb it. In a certain period, this process caused surface sliming of the samples with more negative Si-O bonds, Al-O broken bonds, and amphoteric Al-OH bonds occurring on the surface, thus increasing its negative electricity and leading to an increase in the absolute value of the Zeta potential of the sample surface. As the leaching time proceeded, more Mg^{2+} entered the particle surface. Rare earth ore particles were slimed into fine particles, accelerating the dissolution of inorganic salts inside the solution and ionizing Ca^{2+} and other impurity cations. However, these cations had sufficient time to adsorb on the particle surface over time to compress the double surface layer and reduce the absolute value of the Zeta potential on the surface of rare earth particles. This was why the absolute value of Zeta potential on the particle surface of rare earth samples increased first and then decreased with time in the middle leaching stage. The value of samples in the high-concentration magnesium sulfate solutions had an upward trend in the later leaching stage. It may be that the presence of more cations leads to the reverse adsorption of RE^{3+} , the increase of electrostatic repulsion between particles and double layer thickness, and then the increasing trend of the absolute value curve of Zeta potential.

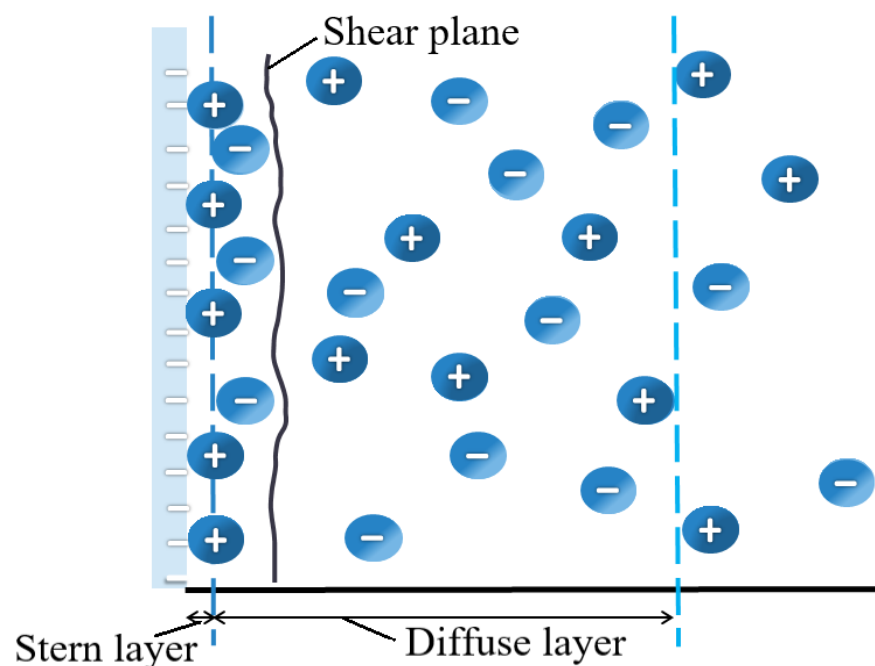


Figure 3. Diagram of electric double-layer structure.

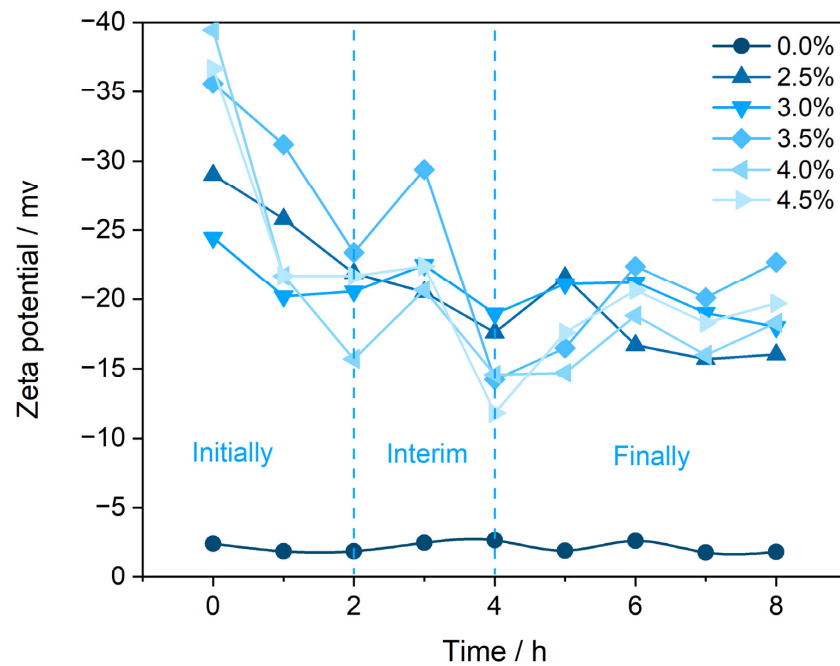


Figure 4. Effect of the concentration of leaching agent on Zeta potential of rare earth particles during the leaching process.

Preparing magnesium sulfate solutions with pH 2, 3, 4, 5, 6 and mass concentration of 3.5% for column leaching experiment. As presented in Figure 5, when magnesium sulfate solutions with different pH are used for leaching, the absolute value of Zeta potential on the surface of rare earth particles decreases with the leaching time going on. When the pH of the solution is 3, the change of Zeta potential reaches the maximum, decreasing by 41.04%. In the early leaching stage, the absolute value of Zeta potential tended to decrease. In the middle stage, the overall change increased and then dropped sharply. In the third hour, the absolute value appeared at a peak. During 3–4 h, the value declined sharply. In the later stage, the value increased gradually, and the overall change was relatively gentle. Due to the strong hydrophobicity of the surface of rare earth ore, the ore particles in solution agglomerate and wrap the clay particles inside, which hinders the hydration of clay particles, resulting in a thinner electric double layer on the surface of particles. The absolute value of Zeta potential on the particle surface decreased in the early leaching stage. There were abundant negative silicon-oxygen bonds and aluminum-oxygen broken bonds, as well as amphoteric Al-OH bonds on the surface and end faces of rare earth ore particles, forming vast amounts of Al-OH, Si-OH, H^+ , and OH^- as their positioning ions and determining the surface charge of rare earth ore particles. In the middle leaching stage, the reason that Zeta potential increased and then decreased was that the number of negative silicon-oxygen bonds and aluminum-oxygen broken bonds increased, increasing the negative charge on the particle surface, i.e., increasing the absolute value of Zeta potential. In an acid medium, H^+ neutralized with OH^- on the surface of particles, compressing the electric double layer on the surface of rare earth ore particles so that its Zeta potential decreased. In the later stage of leaching, the electrostatic repulsion between particles and the thickness of the double layer increased, leading to an increasing trend of the absolute value curve of Zeta potential.

3.2. Effect of Leaching Agent Concentration on Pore Structure of Orebody

During the leaching process of ionic rare earth ore, ion exchange reaction, and seepage occur inside the ore sample, resulting in a change of internal micropore structure and pore size. Nuclear magnetic resonance imaging technology was used to test and analyze the change in the micropore structure. As Figure 6 shows, the porosity of samples leached in

pure H₂O agent changes slightly within the range of 0.8%. The main cause of such change came from the permeation effect of the leaching process. The particles inside the samples caused local pore fluctuations under the effect of seepage. As the seepage continued, the particles, driven by the fluid, were separated from the parent body, resulting in the continuous development of pore structure and, thus, a slight increase in overall porosity. From Figure 7, it can be seen that the T2 map change curve of pure H₂O coincides during leaching, and the change trend is consistent. The overall performance was to rise first and then decrease in area A, rise to the peak in area B, and gradually decrease and finally approach zero in area C. Therefore, it can be concluded that the pore proportion of area A was relatively small, area B was the largest, and area C was second.

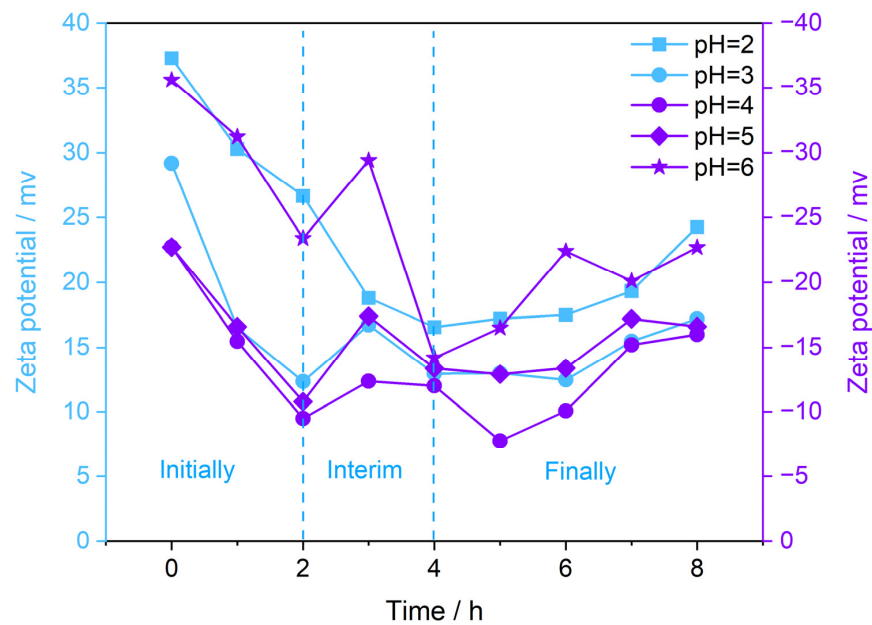


Figure 5. Influence of leaching agent pH on surface Zeta potential of rare earth particles during leaching.

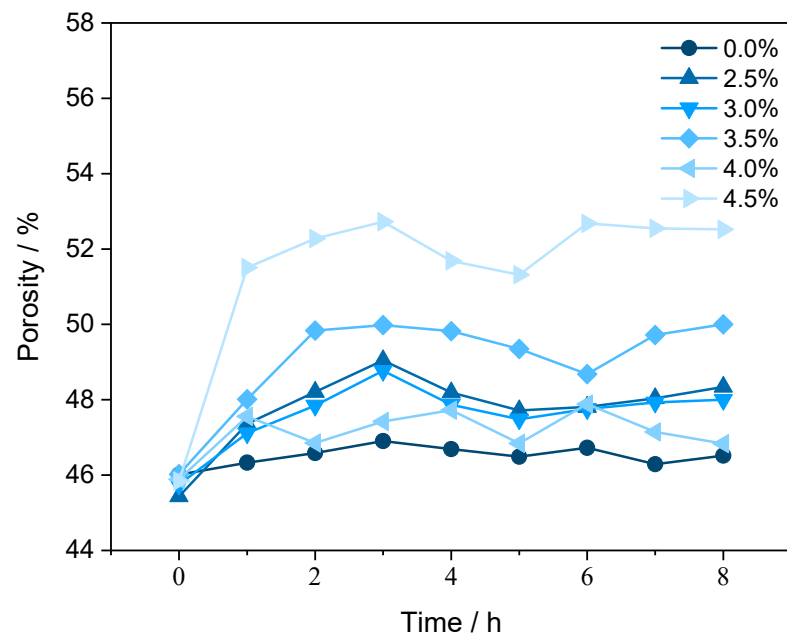


Figure 6. Porosity changing curve of samples with different concentrations of leaching agents in the leaching process.

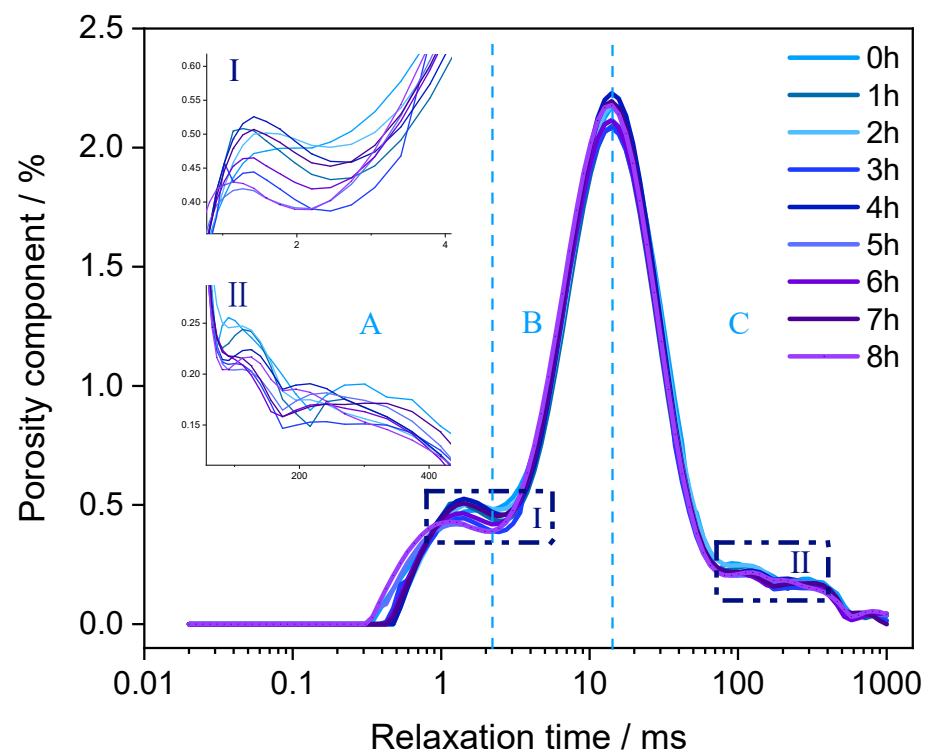


Figure 7. Evolution curve of T2 map in pure H₂O leaching process.

As shown in Figure 6, the effect of magnesium sulfate solution as a leaching agent on the pore structure of the orebody is greater than that of pure H₂O. The porosity of samples leached with different concentrations of magnesium sulfate solution increased first, decreased during the leaching time, and finally increased slowly, though the increase varied. During the leaching process, the porosity of the samples in 4.5% magnesium sulfate solution was the largest. Its porosity increased by 14.57% and reached the maximum of 52.725% after 3 h of column leaching. The increase was followed by the samples in the 3.5% magnesium sulfate solution, which had an 8.64% increase in porosity with a maximum of 50.000% after 8 h of leaching. The porosity of the remaining test groups of magnesium sulfate solutions showed little change. The porosity of samples increased during the leaching process, mainly because the previously unconnected pores in the samples were interconnected by the deionized water-saturated sample in the early stage. When the magnesium sulfate solution was used for leaching, the Mg²⁺ in the leaching agent exchanged ions with RE³⁺ on the surface of clay minerals. In this reaction, a large amount of Mg²⁺ was adsorbed to the diffusion electric double layer under the electrostatic interaction, breaking the balance of the double layer. At the same time, the physical seepage in the solution changed the pore structure.

According to the range of pore radius, the pores are divided into 4 categories: pores with a size range of 0–0.24 μm are called small pores, 0.24–0.65 μm as medium pores, 0.65–10 μm as large pores, and greater than 10 μm as extra-large pores.

Figure 8 shows the pore distribution of samples leached with magnesium sulfate solutions of different concentrations during the leaching process. The pore radius of the sample leached with pure H₂O changed little throughout the process. In 0–8 h, the size of small pores increased by 7.11%, large pores decreased by 13.29%, while that of other groups was basically unchanged. The result implicated that the seepage effect had the greatest influence on the large pores with a size between 0.65–10 μm and that the large pores can be transformed into small pores with a size of 0–0.24 μm. The change of pore size in 3.5% and 4.5% magnesium sulfate solutions was nearly the same. The overall performance showed that the small pores decreased and the large pores increased during the leaching time. The change in the 3.5% magnesium sulfate solution was particularly obvious. In 0–8 h, the size

of small pores decreased by 43.87%, large pores increased by 55.40%, and the medium pores increased first and then decreased. Meanwhile, the thickness of the electronic double layer and the diffusion layer of clay minerals increased, and the small pores evolved towards the large and extra-large pores. The evolution inside the samples affected the physical seepage of the leaching agent. The characteristics of the remaining magnesium sulfate solutions were similar. When a strong ion exchange reaction occurred, the internal pores inside the samples were mainly small and medium, and the former increased rapidly. The proportion of large and extra-large pores was small, and their number decreased. This was because the electrostatic repulsion between particles was reduced, and the van der Waals force played a leading role, under which the particles were adsorbed on the surface of pores inside the orebody, resulting in the evolution of large pores into small ones.

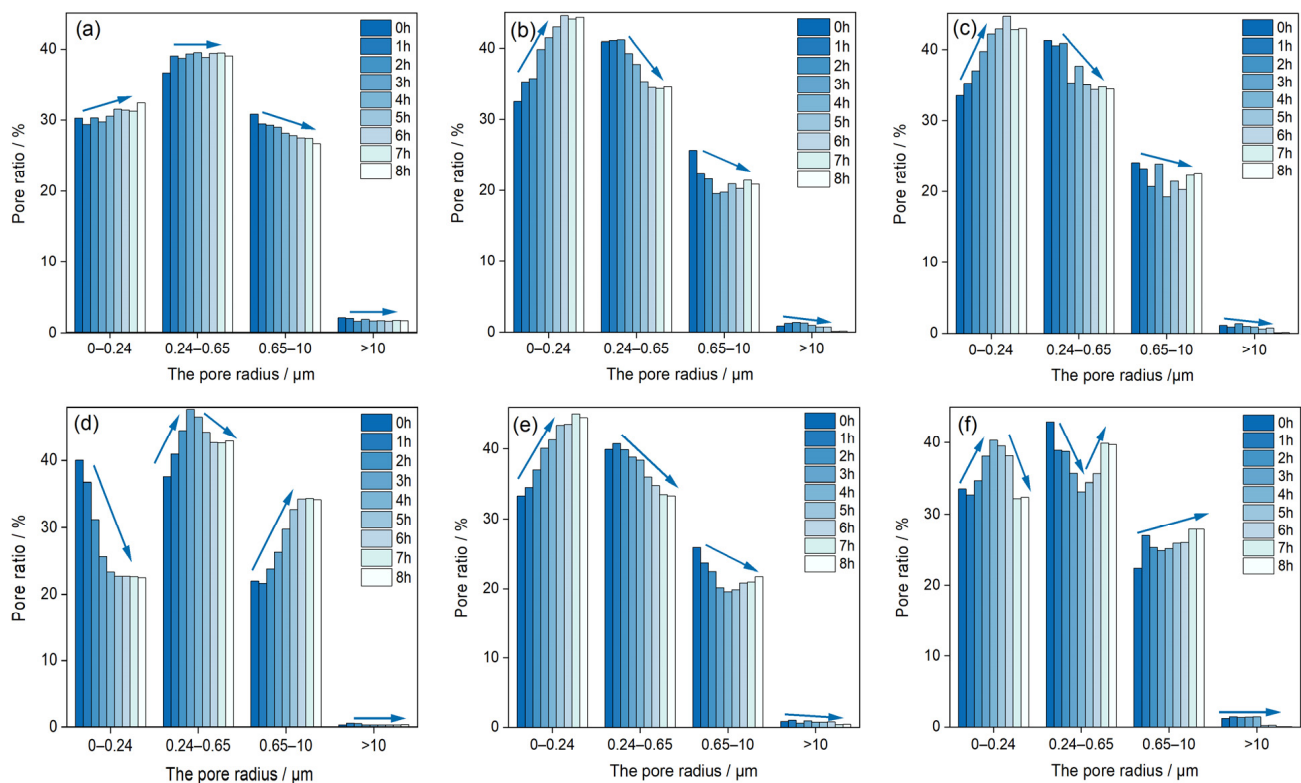


Figure 8. Internal pore distribution of samples with different concentrations of magnesium sulfate solution in the leaching process: (a) 0.0%; (b) 2.5%; (c) 3.0%; (d) 3.5%; (e) 4.0%; (f) 4.5%.

By comparing the pore proportion distribution of the six groups of samples in the leaching process, the sample with 3.0% magnesium sulfate solution was taken as a reference. The pore proportions of the other five groups were subtracted from that of the reference group to determine the difference in pore numbers in the leaching process with different concentrations of magnesium sulfate solutions, as shown in Figure 9. It can be seen from Figure 9a that there are more large and extra-large pores inside the orebody in the pure H_2O leaching group, and more small pores in the 3.0% magnesium sulfate solution sample. As shown in Figure 9b,d, the internal pore proportion of 2.5% and 4.0% magnesium sulfate solutions is roughly the same as that of the 3.0% solution sample, with a difference fluctuation range from -4.365% to $+3.927\%$. Compared with samples leached with 3.0% solution, the number of medium pores increased while large pores decreased at the 4th hour in the 2.5% and 4.0% groups. Combined with Figure 4, it can be seen that the absolute value of Zeta potential was the smallest at the 4th hour when the electrostatic repulsion between particles was reduced. The orebody particles were adsorbed on the surface of coarse particles or pores inside the orebody under the van der Waals force, causing an increase in the number of medium pores and a decrease in the large pores. As seen in Figure 9c,e, there are more

large pores inside the samples leached with 3.5% and 4.5% magnesium sulfate solutions and more small pores in the 3.0% solution sample. According to the comparative analysis of the 6 groups of samples, the small and extra-large pores accounted for the majority of the samples leached with a 3.0% magnesium sulfate solution, while the medium and large pores were relatively small.

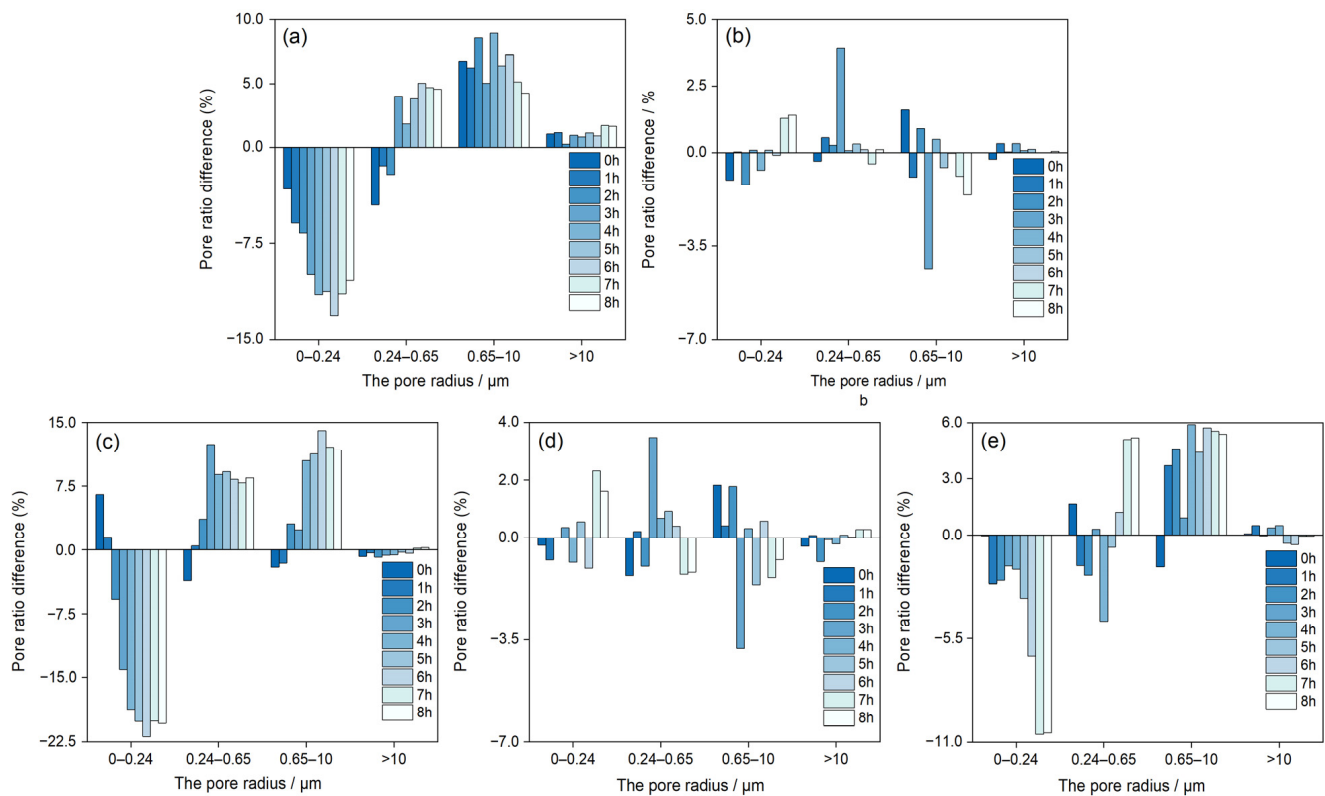


Figure 9. Comparative distribution of differences between different pore structures of samples leached with different concentrations of magnesium sulfate solutions: (a) difference of pore proportion between 0.0% and 3.0% solutions; (b) difference of pore proportion between 2.5% and 3.0% solutions; (c) difference of pore proportion between 3.5% and 3.0% solutions; (d) difference of pore proportion between 4.0% and 3.0% solutions; (e) difference of pore proportion between 4.5% and 3.0% solutions.

3.3. Effect of pH of Leaching Agent on Pore Structure of Orebody

Figure 10 shows the porosity change of samples of magnesium sulfate solutions with different pH in the leaching process. During the leaching process of magnesium sulfate solutions with different pHs, the porosity increased and then decreased during the leaching time and finally increased gradually, though the increase varied. Throughout the process, the porosity of magnesium sulfate solution with pH = 6 was the largest, changing by 3.978% and increasing by 8.64%. The increase of the solution with pH = 5 was the smallest at 6.09%, and the change of porosity was 2.271%. After 2h of leaching, the sample of magnesium sulfate solution with pH = 2 reached the maximum value of 50.348%, with an increase of 9.38%, the largest increase in porosity. The porosity of samples increased during the leaching process, mainly because the previously unconnected pores in the samples were interconnected by the deionized water-saturated sample in the early stage. When the magnesium sulfate solution was used for leaching, the Mg^{2+} in the leaching agent exchanged ions with RE^{3+} on the surface of clay minerals. In this reaction, a large amount of Mg^{2+} was adsorbed to the diffusion electric double layer under the electrostatic interaction, breaking the balance of the double layer. At the same time, the physical seepage in the solution changed the pore structure. As the acidity of the magnesium sulfate solution increased, the $-OH$ group in some mineral components of the samples dissolved, resulting

in the deposition of fine particles and slowing down of the porosity change. Meantime, the increase of hydrogen ions in the leaching solution thickened the double layer of clay minerals, leading to the change of internal pores of samples and a gradual increase of the number of large pores with the leaching time going on.

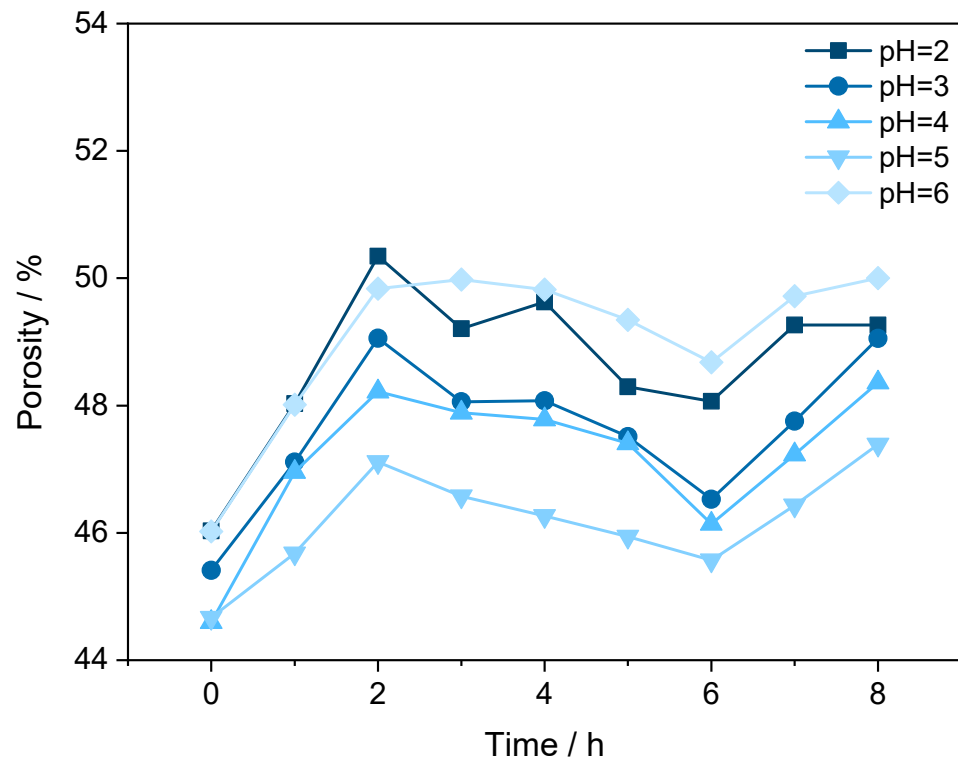


Figure 10. Curve of porosity of samples with pH of different leaching agents.

Figure 11 shows the pore distribution of samples leached with magnesium sulfate solutions with different pHs during the leaching process. The overall performance indicated that the number of small and extra-large pores decreased while the number of medium and large pores increased. As seen in the pore distribution of samples with pH = 2, pH = 4, and pH = 6, the evolution characteristics of the three samples were consistent, showing that the small and medium pores accounted for the majority and that the number of internal pores with sizes of less than 0.24 μm decreased, while medium and large pores with sizes between 0.24–10 μm increased. According to the pore distribution of the sample with pH = 3 and pH = 5, in 0–2 h, the number of small pores increased and medium and large pores decreased, while in 3–8h, the small pores decreased and medium and large pores increased. By comparing the pore distribution of the five sample groups, taking the sample of magnesium sulfate solution with pH = 3 as the contrast reference, and subtracting the pore proportion of the reference group from that of the other four groups, the difference in pore content of the magnesium sulfate solutions with different pHs in the leaching process was determined, as shown in Figure 12. In Figure 12a,b,d, during the leaching process of magnesium sulfate solutions with pH = 2, pH = 4, and pH = 6, there are more medium, large, and extra-large pores. In the solution with pH = 3, there are more small pores. It can be seen in Figure 12c that the pore proportion of a solution with pH = 5 is roughly the same as that of pH = 3, fluctuating from -1.845% – $+2.604\%$, and that the small and medium pores are relatively few. According to Figure 5, the absolute values of the Zeta potential are nearly the same, with similar curves. Meanwhile, the interaction force between particles had the same effect on the sample interiors.

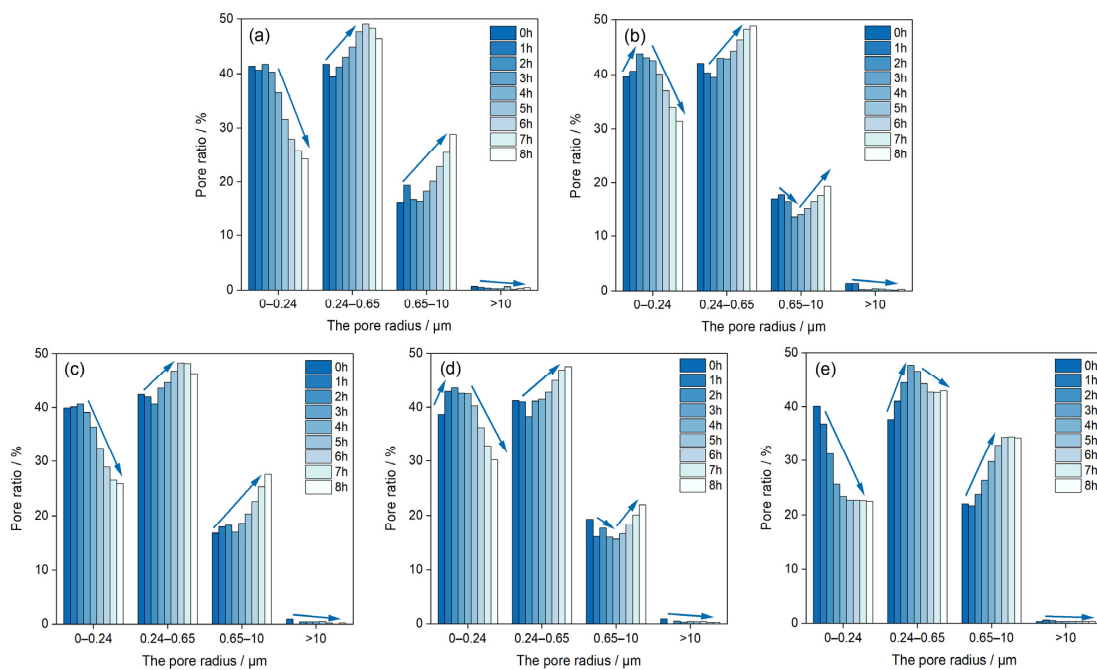


Figure 11. Distribution of internal pores of samples in the process of leaching with magnesium sulfate solutions with different pH: (a) pH = 2; (b) pH = 3; (c) pH = 4; (d) pH = 5; (e) pH = 6.

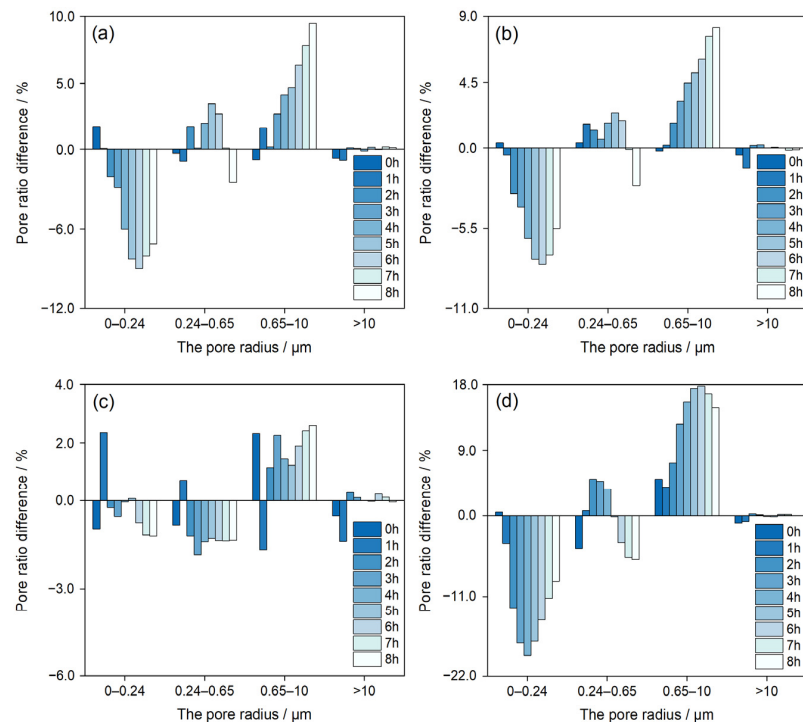


Figure 12. Comparative distribution of differences of different Pore structure of samples during the leaching process of magnesium sulfate solutions with different pH: (a) difference of pore proportion between solutions with pH = 2 and pH = 3; (b) difference of pore proportion between solutions with pH = 4 and pH = 3; (c) difference of pore proportion between solutions with pH = 5 and pH = 3; (d) difference of pore proportion between solutions with pH = 6 and pH = 3.

4. Conclusions

Using the method of indoor simulated column leaching of ionic rare earth ores, the influence of magnesium sulfate solutions with different concentrations and pHs on the

evolution of the pore structure of the orebody during the leaching process is systematically studied. The overall process of leaching is a process of seepage, ion exchange, ion migration, and pore structure evolution. The main conclusions are as follows:

1. In the leaching process of rare earth samples with pure H₂O, the curve of the change of Zeta potential on the surface of rare earth ore particles is nearly a straight line. The particles inside the sample cause local pore fluctuation under the effect of seepage. The porosity changes slightly within 0.80%, which has little impact on the pore structure of the orebody;
2. In the leaching process of magnesium sulfate solution with different mass percent concentrations, the absolute value of Zeta potential on the surface of rare earth ore particles decreases with the leaching time going on. When the solution with a concentration of 4.0% is used as a leaching agent, the change of the Zeta potential reaches the maximum, reducing by 53.60%. The curve of the Zeta potential change of samples leached with high concentrations of magnesium sulfate solutions fluctuates greatly, while that of low-concentration solutions is relatively gentle. The porosity increases first, then decreases, and finally slowly increases during the leaching time. The internal pores are mainly small and medium. During the leaching time, the number of small and large pores increases in the samples with 3.5% and 4.5% solutions. In the samples with the other concentrations, the number of small pores increases rapidly while the number of large and extra-large pores is small and decreases;
3. In the leaching process of magnesium sulfate solutions with different pH, the absolute value of Zeta potential on the surface of rare earth ore particles decreases during the leaching time. In the later stage of the process, the value shows a slightly increasing trend. When the magnesium sulfate solution with pH = 3 is used as a leaching agent, the change of Zeta potential reaches the maximum, reducing by 41.04%. The porosity increases first and then decreases, and finally slowly increases with time. The internal pore structure of the samples generally shows that the number of small and extra-large pores decreases while the number of medium and large pores increases;
4. When magnesium sulfate solutions with different concentrations and pH are used for leaching, a chemical replacement reaction occurs between Mg²⁺ and RE³⁺, resulting in a change in the thickness of the electric double layer and the breaking of the balance between the van der Waals force and electric double layer repulsion of fine particles and soil surface. The reaction also causes the agglomeration, dispersion, and dynamic desorption transformation of fine particles, leading to the evolution of the microscopic pore structure of the orebody during the leaching process.

Author Contributions: Conceptualization, Z.G. and Y.R.; methodology, Z.G.; software, Z.G., R.X. and Z.Y.; validation, L.S.; data curation, Z.G.; writing—original draft preparation, Z.G. and Y.R.; writing—review and editing, Z.G., Y.R. and L.S.; visualization, L.S., R.X. and Z.Y.; supervision, Y.R.; project administration, Y.R.; funding acquisition, Y.R. and L.S. All authors have read and agreed to the published version of the manuscript.

Funding: This research was supported by the National Natural Science Foundation of China (51964014) and the Education Department of Jiangxi Province (GJJ209414).

Data Availability Statement: Not applicable.

Acknowledgments: Thanks for the great effort by the editors and reviewers.

Conflicts of Interest: The authors declare no conflict of interest.

References

1. Zhou, L.B.; Wang, X.J.; Huang, C.G.; Wang, H.; Ye, H.C.; Hu, K.J.; Zhong, W. Development of pore structure characteristics of a weathered crust elution-deposited rare earth ore during leaching with different valence cations. *Hydrometallurgy* **2021**, *201*, 105579. [[CrossRef](#)]
2. Nie, W.R.; Zhang, R.; He, Z.Y.; Zhou, J.; Wu, M.; Xu, Z.G.; Chi, R.A. Research progress on leaching technology and theory of weathered crust elution-deposited rare earth ore. *Hydrometallurgy* **2020**, *193*, 105295. [[CrossRef](#)]

3. Moldoveanu, G.A.; Papangelakis, V.G. An overview of rare-earth recovery by ion-exchange leaching from ion-adsorption clays of various origins. *Miner. Mag.* **2016**, *80*, 63–76. [[CrossRef](#)]
4. Huang, X.W.; Long, Z.Q.; Li, H.W.; Ying, W.J.; Zhang, G.C.; Xue, X.X. Development of rare earth hydrometallurgy technology in China. *J. Rare Earths* **2005**, *23*, 1–4. [[CrossRef](#)]
5. Moldoveanu, G.A.; Papangelakis, V.G. Recovery of rare earth elements adsorbed on clay minerals: I. Desorption mechanism. *Hydrometallurgy* **2012**, *117*, 71–78. [[CrossRef](#)]
6. Yan, H.S.; Liang, T.M.; Liu, Q.S.; Qiu, T.S.; Ai, G.H. Compound leaching behavior and regularity of ionic rare earth ore. *Powder Technol.* **2018**, *333*, 106–114. [[CrossRef](#)]
7. Hu, J.; Shen, Y.; Wang, X. The effect of ionic strength and pH conditions on the release, deposition and dispersibility behaviors of natural soil colloid. *Ecol. Environ. Sci.* **2009**, *18*, 629–637.
8. Tian, J.; Tang, X.K.; Yin, J.Q.; Chen, J.; Luo, X.P.; Rao, G.H. Enhanced leachability of a lean weathered crust elution-deposited rare-earth ore: Effects of Sesbania gum filter-aid reagent. *Metall. Mater. Trans. B* **2013**, *44*, 1070–1077. [[CrossRef](#)]
9. Zhang, Z.Y.; Xu, Z.G.; Wu, M.; Zhang, T.T.; Li, Q.; Chi, R.A. Study on leaching of rare earth from weathered crust elution-deposited rare earth ore with complex ammonium agents. *Nonferrous Metals (Extr. Metall.)* **2013**, *4*, 32–35.
10. Kyle, J.R.; Ketcham, R.A. Application of high resolution X-ray computed tomography to mineral deposit origin, evaluation, and processing. *Ore. Geol. Rev.* **2015**, *65*, 821–839. [[CrossRef](#)]
11. Munkholm, L.J.; Heck, R.J.; Deen, B. Soil pore characteristics assessed from X-ray micro-CT derived images and correlations to soil friability. *Geoderma* **2012**, *181*, 22–29. [[CrossRef](#)]
12. Luo, X.P.; Zhang, Y.B.; Zhou, H.P.; He, K.Z.; Zhang, B.Y.; Zhang, D.M.; Xiao, W.J. Pore structure characterization and seepage analysis of ionic rare earth orebodies based on computed tomography images. *Int. J. Min. Sci. Technol.* **2022**, *32*, 411–421. [[CrossRef](#)]
13. Kodali, P.; Dhawan, N.; Depci, T.; Lin, C.L.; Miller, J.D. Particle damage and exposure analysis in HPGR crushing of selected copper ores for column leaching. *Miner. Eng.* **2011**, *24*, 1478–1487. [[CrossRef](#)]
14. Bezaatpour, J.; Fatehifar, E.; Rasoulzadeh, A. Coarse-grained geological porous media structure modeling using heuristic algorithm and evaluation of porosity, hydraulic conductivity, and pressure drop with experimental results. *Environ. Earth Sci.* **2021**, *80*, 1–14. [[CrossRef](#)]
15. Wang, X.J.; Zhuo, Y.L.; Zhao, K.; Zhong, W. Experimental measurements of the permeability characteristics of rare earth ore under the hydro-chemical coupling effect. *RSC Adv.* **2018**, *8*, 11652–11660. [[CrossRef](#)] [[PubMed](#)]
16. Wang, X.J.; Zhuo, Y.L.; Deng, S.Q.; Li, Y.X.; Zhong, W.; Zhao, K. Experimental research on the impact of ion exchange and infiltration on the microstructure of rare earth orebody. *Adv. Mater. Sci. Eng.* **2017**, *2017*, 1–8. [[CrossRef](#)]
17. Zhao, K.; Zhuo, Y.L.; Wang, X.J.; Zhong, W. Aggregate evolution mechanism during ion-adsorption rare earth ore leaching. *Adv. Mater. Sci. Eng.* **2018**, *2018*, 1–10. [[CrossRef](#)]
18. Caron, J.; Espindola, C.R.; Angers, D.A. Soil structural stability during rapid wetting: Influence of land use on some aggregate properties. *Soil Sci. Soc. Am. J.* **1996**, *60*, 901–908. [[CrossRef](#)]
19. Curtin, D.; Steppuhn, H.; Selles, F. Effects of magnesium on cation selectivity and structural stability of sodic soils. *Soil Sci. Soc. Am. J.* **1994**, *58*, 730–737. [[CrossRef](#)]
20. Baumann, T.; Toops, L.; Niessner, R. Colloid dispersion on the pore scale. *Water Res.* **2010**, *44*, 1246–1254. [[CrossRef](#)]
21. Olphen, V.H. An introduction to clay colloid chemistry. *Soil Sci.* **1964**, *97*, 290. [[CrossRef](#)]
22. Helmholtz, H. Über einige Gesetze der Vertheilung elektrischer Ströme in Körperlichen Leitern, mit Anwendung auf die thierischelektrischen Versuche. *Ann. Phys.* **1853**, *165*, 211. [[CrossRef](#)]
23. Gouy, M. Sur la constitution de la charge électrique à la surface d'un électrolyte. *J. Phys. Theor. Appl.* **1910**, *9*, 457–468. [[CrossRef](#)]
24. Zheng, W.B.; Hu, X.L.; Tannant, D.D.; Zhou, B. Quantifying the influence of grain morphology on sand hydraulic conductivity: A detailed pore-scale study. *Comput. Geotech.* **2021**, *135*, 104147. [[CrossRef](#)]
25. Shi, L.; Rao, Y.Z.; Wang, D.; Zhang, M.D.; Huang, T. A Capillary Model for Predicting Saturated Hydraulic Conductivity of Ion-Adsorption Rare Earth Ore Based on Improved Kozeny–Carman Equation. *Geofluids* **2022**, *2022*, 1–10. [[CrossRef](#)]
26. Liu, Y.; Li, Z.; Guo, L.; Kang, W.; Zhou, Y. Pore characteristics of soft soil under triaxial shearing measured with NMR. *Chin. J. Rock Mech. Eng.* **2018**, *37*, 1924–1932.
27. Bissonnais, Y.L. Aggregate stability and assessment of soil crustability and erodibility: I. Theory and methodology. *Eur. J. Soil Sci.* **1996**, *47*, 425–437. [[CrossRef](#)]
28. Hu, F.N.; Xu, C.Y.; Li, H.; Li, S.; Yu, Z.H.; Li, Y.; He, X.H. Particles interaction forces and their effects on soil aggregates breakdown. *Soil Tillage Res.* **2015**, *147*, 1–9. [[CrossRef](#)]
29. Hu, Y. Surface zeta potential and surface absorption—A theoretical explanation of the rule of coagulation. *Chin. J. Struct. Chem.* **1992**, *11*, 447–452.

Disclaimer/Publisher's Note: The statements, opinions and data contained in all publications are solely those of the individual author(s) and contributor(s) and not of MDPI and/or the editor(s). MDPI and/or the editor(s) disclaim responsibility for any injury to people or property resulting from any ideas, methods, instructions or products referred to in the content.